A mesocosm experiment coupled with optical measurements to assess the fate and sinking of atmospheric particles in clear oligotrophic waters

Matthieu Bressac, Cécile Guieu, David Doxaran, François Bourrin, Grigor Obolensky & Jean-Michel Grisoni

Geo-Marine Letters
An International Journal of Marine Geology

ISSN 0276-0460

Geo-Mar Lett
DOI 10.1007/s00367-011-0269-4

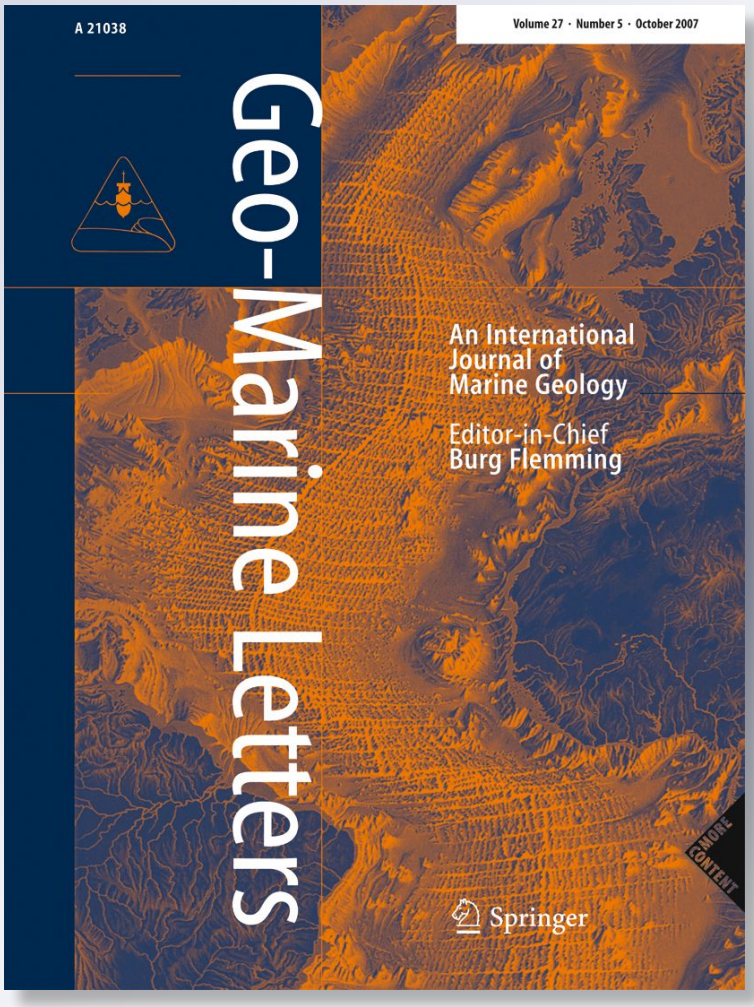

Springer

Geo-Mar Lett
DOI 10.1007/s00367-011-0269-4

ORIGINAL

A mesocosm experiment coupled with optical measurements to assess the fate and sinking of atmospheric particles in clear oligotrophic waters

Matthieu Bressac · Cécile Guieu · David Doxaran · François Bourrin · Grigor Obolensky · Jean-Michel Grisoni

Received: 15 April 2011 / Accepted: 24 November 2011

Abstract It has recently been postulated that lithogenic particles such as Saharan dust strongly influence particulate organic carbon export to the deep ocean by acting as mineral ballast. However, our understanding of the processes involved remains scant. In the present study, optical measurements were performed to monitor variations in the concentration, composition and size distribution of particles in suspension within the water column after simulating a Saharan dust event in very clear Mediterranean waters off Corsica in June 2010. A new methodology set up in large mesocosms proved very successful in this regard. Values obtained simultaneously from three instruments (WetLabs ECO-BB3, WetLabs ac-9, Sequoia Scientific LISST-100) provided evidence that (1) part of the Saharan dust pool has a rapid settling velocity (~24–86 m day^{-1}), (2) particulate export following a dust event is a nonlinear multi-step process and (3) export is controlled in part by the formation of organic-mineral aggregates. This experimental study provides the first insight of the complex export processes occurring after a dust event involving both physical and biogeochemical forcings in clear oligotrophic waters.

Responsible guest editor: O. Mikkelsen

Electronic supplementary material The online version of this article (doi:10.1007/s00367-011-0269-4) contains supplementary material, which is available to authorized users.

M. Bressac (✉)
ACRI-ST,
BP 234, 06904 Sophia-Antipolis, France
e-mail: bressac@obs-vlfr.fr

M. Bressac · C. Guieu · D. Doxaran · G. Obolensky
CNRS-INSU, Université Pierre et Marie Curie-Paris 6,
UMR 7093, Laboratoire d'Océanographie de Villefranche/Mer,
Observatoire Océanologique,
06230 Villefranche-sur-Mer, France

F. Bourrin
Université de Perpignan, CEFREM, CNRS-UPVD, UMR 5110,
52 avenue Paul Alduy,
66860 Perpignan, France

J.-M. Grisoni
Observatoire Océanologique de Villefranche/Mer, CNRS,
Université Pierre et Marie Curie-Paris 6,
06230 Villefranche-sur-Mer, France

Introduction

Sporadic high-magnitude Saharan dust deposition occurs over large areas in the Mediterranean Sea (Loÿe-Pilot and Martin 1996; Ternon et al. 2010), and it has long been known that particulate concentrations and fluxes in the upper water column can increase significantly following dust transport and deposition events with a short response time (Buat-Ménard et al. 1989). Recent studies have demonstrated that Saharan dust bring elements of biogeochemical significance to the Mediterranean Sea, such as phosphorus and iron that may alleviate biological limitation during summer (e.g. Bonnet et al. 2005; Ternon et al. 2011). Being the only external source of new nutrients during the period of water column stratification, these inputs can be seen as fertilizing events. Moreover, through the process of aggregation and the ballast effect, atmospheric particles have been postulated to enhance particulate organic carbon

Published online: 23 December 2011

(POC) export to the deep ocean (Hamm 2002; Passow and De La Rocha 2006; Ploug et al. 2008; Ternon et al. 2010). However, in situ parameterizations of links between dust deposition and aggregation processes are lacking and "observations between POC and minerals are needed to test and refine the ballast hypothesis" (De La Rocha et al. 2008).

So far, two approaches have been used to estimate the physical role of lithogenic particles in this context. Several laboratory studies have simulated the sinking of particles, the formation of aggregates and the accumulation of 'ballast minerals' in roller tanks (e.g. Passow and De La Rocha 2006; De La Rocha et al. 2008; Ploug et al. 2010). The other, so-called benchmark approach has attempted to estimate the temporal scales associated with particle fluxes propagating between sediment traps located at various water depths (e.g. Brust et al. 2011). Nevertheless, knowledge on the actual impact of atmospheric deposition and processes involved in material export to the deep ocean remains scant.

The objective of this paper is to determine the fate of Saharan dust when depositing at the ocean surface and associated interactions within the particulate pool during particle transfer to the deep ocean. The work was conducted within the framework of the DUNE (DUst experiment in a low Nutrient, low chlorophyll Ecosystem) project involving the artificial seeding of Saharan dust in large mesocosms. Due to difficulty in directly measuring suspended particulate matter (SPM) concentration at high temporal and spatial resolutions, multiple optical measurements were carried out during the DUNE-2 experiment in the summer of 2010, in the first mesocosm attempt to assess variations in the concentration, composition and size distribution of particles in suspension after simulating a Saharan dust event in very clear Mediterranean waters. Monitoring was done by means of an ECO-BB3 backscattering sensor and an ac-9 photometer, which respectively measure the backscattering coefficient and the light attenuation and absorption coefficients. Furthermore, particle size distributions were evaluated with a laser scattering and transmissometry device (LISST-100). This enabled assessment of the effectiveness and limits of these various optical measurements as tools to parameterize complex processes involved in the sinking of both lithogenic and organic particles following an intense dust event.

Materials and methods

Study area and experimental setup

Oligotrophic conditions

Within the framework of the DUNE project, seven large mesocosms were deployed in Elbo Bay off Corsica (Scandola marine preservation area: 42.374°N, 8.554°E). This coastal area is characterised by oligotrophic conditions in summer and is representative of very clear Mediterranean waters. Uplift of the Ligurian current along the Corsican coast isolates it from more productive waters prevailing in the central Ligurian Sea (Guieu et al. 2010). Artificial seeding took place in June and July 2010. At the beginning of the experiment, chlorophyll a concentrations were typical of oligotrophic systems (0.047 ± 0.010 mg m^{-3}).

Experimental setup

The methodology concerning the DUNE mesocosms is fully described in Guieu et al. (2010). Briefly, each mesocosm has the following dimensions: diameter: 2.3 m, height: 14.7 m, surface area: 4.15 m^2, volume: 52 m^3 (Fig. 1a). They comprised a polyethylene bag and a PVC support, which did not inhibit turbulence generated by swell and currents. The mesocosms ended in a sediment trap (Fig. 1a) from which material was collected every 24 h. Having deployed the main cylindrical part of each mesocosm, it was left open for 24 h to enable water stabilization, after which the conical bottom was attached to the main cylinder.

Saharan dust characteristics and simulation of dust event

The methodology to produce the dust used in the present study is fully described in Guieu et al. (2010). Briefly, soil was collected in an aerosol source region in southern Tunisia. Dust particles were dominated by quartz (40%), calcite (30%) and clays (25%). The finest dust fraction (<20 μm)

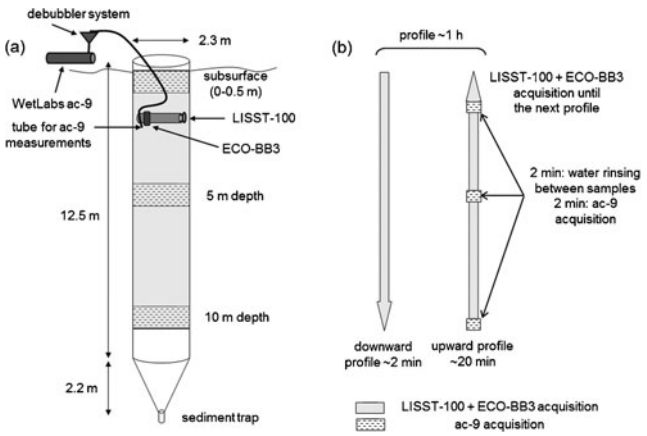

Fig. 1 **a** Schematic view of the mesocosm and the optical package (one LISST-100 deployed horizontally and one ECO-BB3 deployed vertically). **b** Schematic of profiles realized inside and outside the mesocosm from 0 to 10 m depth, taken every hour and then continuously recorded at the subsurface. A tube fixed onto the optical package pumped seawater at 0.25, 5 and 10 m depths through the ac-9 sensor every hour (*min* minutes)

was separated from the bulk soil samples by grinding and dry-sieving; larger particles are rapidly removed during atmospheric transport (Maring et al. 2003). The particle number size distribution of the dust peaked at 0.1 μm, and 99% of the particles were smaller than 1 μm in diameter. Based on Stokes' law, these characteristics imply that the dust particles would have very slow settling velocity in seawater.

The dust solution was prepared with 41.5 g dust in 2 L ultrapure water, and quickly spread at the surface of the mesocosm using a sprayer to mimic a wet deposition event with a flux of 10 g m^{-2}. This represents a realistic event observed in the north-western Mediterranean Sea (e.g. Ternon et al. 2010), where Saharan dust events are associated mainly to wet deposition (Loÿe-Pilot and Martin 1996). In all, seven mesocosms were deployed. Three seeded (triplicate treatment with dust addition) and three unseeded (triplicate control) mesocosms served for the monitoring of biogeochemical parameters; these data are not reported in the present publication. The seventh mesocosm was also seeded and served for the deployment of optical instruments, with data acquisition from a floating platform moored close by.

Sampling strategy and field measurements

Sampling plan

The DUNE-2 experiment lasted 14 days, from 26 June to 09 July 2010. Two artificial seedings were successively conducted (with the same flux of dust) 7 days apart in the same mesocosms. Only the optical measurements made before and during 3 days after the first seeding experiment are presented in this paper (25–28 June 2010). The sampling plan is detailed in Table 1 available online in the electronic supplementary material. Briefly, optical data were recorded inside and outside the mesocosm 1 day before seeding, in order to determine the initial conditions (time 0). Sampling was in two periods, each corresponding to profiles performed every hour: (1) the first 31 h of the experiment (two daytime periods and one night of continuous measurements) served for assessment of short-term processes involved in particulate export; (2) the subsequent period comprises data acquired continuously between hours 47 and 54. The optical properties of the water column outside of the mesocosm were measured before and at ~31, 47 and 54 h after seeding, in order to check for possible modifications not related to seeding.

Sampling protocol

Field measurements were carried out using an optical package comprising an ECO-BB3 (WetLabs Inc.) backscattering sensor, a LISST-100 type B device (Sequoia Scientific Inc.) and a tube connected to an ac-9 photometer (WetLabs Inc.) for discrete measurements (Fig. 1a). The fact that these three components were set up at the same water level enabled meaningful comparisons. A peristaltic pump was connected to the tube attached to the profiling package in order to collect seawater for the ac-9 measurements. The optical package was deployed along vertical profiles from 0 to 10 m depth at a speed of 10 cm s^{-1} at the centre of the bag, in order to minimize perturbation inside the mesocosm when profiling.

Vertical profiles consisted of continuous measurements between the subsurface and 10 m depth with the ECO-BB3 and LISST-100 sensors. While these two sensors were still in acquisition mode, discrete measurements were performed with the ac-9 photometer on water pumped at 0.25, 5 and 10 m depths (Fig. 1b). Prior to each measurement, the tube and the ac-9 sensors were rinsed. The pumped seawater was then passed through a funnel in order to remove air bubbles, and the data recorded during at least 2 min. Vertical profiles were performed every hour and lasted approximately 20 min. During the remaining 40 min, measurements were carried out continuously at 0.5 m depth with the ECO-BB3 and LISST-100 sensors (both at 1 Hz frequency). The outside profiles (control) were performed in the same way.

Parameters monitored

The particulate backscattering coefficient (b_{bp}, m^{-1}) was obtained from light backscattered at 117° ($\beta(117°)$, m^{-1} sr^{-1}) measured with the ECO-BB3 at 440, 532 and 660 nm. The LISST-100 type B measures the beam attenuation coefficient at 670 nm along a path length of 5 cm and light scattering at 32 angles in the forward directions, from which is derived the particle size distribution (PSD) between 1.25 and 250 μm. The light absorption and attenuation coefficients were simultaneously measured at three visible (440, 555 and 630 nm) and six near-infrared (715, 730, 750, 767, 820 and 870 nm) wavelengths with the ac-9 along a path length of 10 cm.

Physical parameters

Salinity was measured with a salinometer on samples collected at 5 m depth inside and outside the mesocosm. The values remained constant during the duration of the experiment: PSU=37.96±0.01 (C. Ridame, personal communication). Depth profiles of seawater temperature (accuracy: 0.1°C) were also ran continuously by auxiliary sensors on the LISST-100.

Measurement corrections and data analysis

Measurement corrections

ECO-BB3 sensor

The ECO-BB3 sensor was calibrated by the manufacturer before the experiment. Backscattering data were averaged within 1 m depth bins. Correction for absorption losses along the photon path length was applied to the measured β_{raw} (m^{-1} sr^{-1}) signal (WetLabs ECO BB User's Guide, version 2010):

$$\beta_a(117^\circ, a=0) = \beta_{raw}(117^\circ, a)\ \exp\ (0.0391a) \quad (1)$$

where a is the absorption coefficient (m^{-1}) measured with the ac-9 photometer. This correction for absorption losses proved to be very small over the entire experiment (systematically <1% of the measured raw coefficient; data not shown), as already reported by Loisel et al. (2007) at 650 nm. Because the absorption coefficient was measured only at 0.25, 5 and 10 m depths with the ac-9 sensor, we decided to keep the measured backscattering coefficients uncorrected for absorption losses. The contribution of pure seawater $\beta_{sw}(117°, \lambda)$ was computed as a function of salinity (Morel 1974) and subtracted from the measured signal to obtain the light backscattered at 117° by particles, $\beta_p(117°, \lambda$; WetLabs ECO BB User's Guide, version 2010):

$$\beta_p(117^\circ, \lambda) = \beta_{raw}(117^\circ, \lambda) - \beta_{sw}(117^\circ, \lambda) \quad (2)$$

The particulate backscattering coefficient ($b_{bp}(\lambda)$, m^{-1}) was then derived by using a conversion factor, χ_p, of 1.1 (Boss and Pegau 2001):

$$b_{bp}(\lambda) = 2\pi\chi_p\beta_p(117^\circ, \lambda) \quad (3)$$

LISST-100 type B

The LISST-100 type B measures the transmission coefficient and the volume scattering function of particles along a 5 cm path length using laser diffraction technology. The inversion matrix (Sequoia Scientific User's Guide) enables converting near-forward scattering measured at 32 angles into particle volume concentration, $V(D)$ in µL L^{-1}, in 32 size classes logarithmically spaced within the size range $1.25<D<250$ µm, D being the particle diameter (Agrawal and Pottsmith 2000). Assuming that the particles are spherical, the particle number distribution $N(D)$ in particles L^{-1}, i.e. the number of equivalently sized spherical particles per size class, was calculated as:

$$N(D) = V(D) \Big/ \left[4/3\pi(D/2)^3\right] \quad (4)$$

Because of significant measurement uncertainties at the limits of the size range as a whole, i.e. at the smallest (D= 1.36 µm) and the largest (D=230 µm) size classes (Agrawal and Pottsmith 2000; Agrawal et al. 2008), these two bins were excluded in further size distribution analysis. Blank offsets were measured using Milli-Q water and subtracted from the sample measurements. This correction implies that values reported here do not include light attenuation by water molecules. The change between the transmitted and received intensity, T, can be converted into the particulate beam attenuation coefficient at 670 nm (hereafter denoted $c_p(670)$, m^{-1}) based on the following:

$$c_p(670) = -\ln(T)/L - c_w(670) \quad (5)$$

where L is the path length (m), T the beam transmission and $c_w(670)$ the attenuation coefficient of pure water (m^{-1}). Raw data were recorded at 1 Hz frequency. Processed data were averaged within 1 m depth bins.

ac-9 sensor

The ac-9 measurements were median filtered at each sample depth to exclude spikes caused by rare, remaining air bubbles. The ac-9 sensor was calibrated with Milli-Q water to obtain a reference signal. Measured absorption and attenuation coefficients ($a(\lambda)$ and $c(\lambda)$ respectively) exclude the contribution of water molecules. Corrections for in situ temperature and salinity effects on optical properties of water were applied to c_{raw} and a_{raw} (Pegau et al. 1997; Sullivan et al. 2006). In the near-infrared, temperature correction factors provided by Langford et al. (2001) were used. Residual scattering effects on absorption measurements were corrected according to the 'proportional' method (Zaneveld et al. 1994). The 870 nm wavelength was used as reference, where particle absorption was assumed to be negligible. The three sensors did not completely match in terms of wavelengths; so, ac-9 attenuation data were linearly interpolated to give c_p at 670 nm for comparison with $c_p(670)$ measured with the LISST-100.

Proxies deduced from optical measurements

Saharan dust concentration

As proxy of Saharan dust concentration, b_{bp} was measured at three wavelengths but here only measurements at 660 nm are reported to remain consistent with LISST-100 data (670 nm); indeed, the results at other wavelengths were similar. In addition, measurements performed in the red and near-infrared regions minimize contamination by dissolved substances. Because particles with a high refractive index tend to backscatter light more efficiently than do low-refractive index particles (Twardowsky et al. 2001), mineral particles are recognized as the main contributor to b_{bp}. Based on Mie theory calculations, small nonliving particles

are considered to determine the magnitude of backscattering (Stramski and Kiefer 1991; Ulloa et al. 1994). In this study, where submicron mineral particles were clearly dominant after seeding, b_{bp} was used mainly as proxy of Saharan dust concentration in the 0–10 m water column of the mesocosm.

Particulate concentration

Light attenuation by particles smaller than 0.2 μm is negligible in the red spectral domain (Boss et al. 2009) and it is generally assumed that, as a first approximation, beam attenuation is largely dependant upon particle concentration. The attenuation coefficients measured at 670 nm were therefore considered as particulate beam attenuation. In this paper, particulate attenuation from the LISST-100 and the ac-9 are used as proxies of particulate concentration.

Composition of particle assemblage

The particulate backscattering ratio (ratio of particulate backscattering to scattering coefficients, b_{bp}/b_p) provides information on particle composition because it can be related to the PSD and bulk particulate refractive index (Twardowsky et al. 2001; Boss et al. 2004; Sullivan et al. 2005; Loisel et al. 2007). At 660 nm, Loisel and Morel (1998) demonstrated that the particle attenuation coefficient is due mainly to particle scattering. During our experiment, $a_p(670)$ measured within subsurface waters represents on average a negligible fraction of $c_p(670)$, i.e. ~6±4%. This means that c_p can be considered equivalent to b_p at this wavelength. Consequently, the ratio of the particulate backscattering coefficient to the particulate attenuation ($b_{bp}(660)/c_p(670)$, hereafter referred to as the backscattering ratio) was selected here as a proxy of particle assemblage composition, consistent with the arguments and approaches of, for example, Boss et al. (2004) and Westberry et al. (2010).

Results

Comparison between optical measurements

A very good agreement (slope=1.052, R^2=0.916, N=31) was observed between $c_p(670)$ obtained from the ac-9 data after linear interpolation and $c_p(670)$ measured by the LISST-100 within subsurface waters (Fig. 2a). Nevertheless, comparison between both measurement techniques should be interpreted with care, as these two sets of measurements have not been carried out with the same sampling method. The coefficient of variation of $c_p(670)$ from the ac-9 is higher (0.81) than that of $c_p(670)$ from the LISST (0.63). The LISST-100 used in a profiling mode better captured the fine-scale vertical variability and this dataset presents a higher spatial resolution than the ac-9 data. For these reasons, the $c_p(670)$ signal measured with the LISST-100 was used to estimate the backscattering ratio.

Profiles performed with the optical package constitute a large dataset (N=397) comprising simultaneous measurements of $b_{bp}(660)$ and $c_p(670)$ between 0 and 10 m depth. Figure 2b shows $b_{bp}(660)$ ranging from 0.0014 to 0.057 m^{-1}, and $c_p(670)$ ranging from less than 0.05 to 2.07 m^{-1}. A linear regression analysis exhibits a high coefficient of determination (R^2=0.854, N=397) between these two datasets, supporting the validity of the corresponding backscattering ratio as proxy (see Discussion).

Physical conditions

During the experiment, the seawater temperature inside the mesocosm ranged from 20–23°C (Fig. 3). During the first 25 h, there was no measurable water column stratification due to surface cooling during the night (between 10 and 20 h after seeding). Thereafter, the surface temperature increased slightly, with temperatures ranging from 22.8°C at the surface to 20.4°C at the bottom of the mesocosm. Such stratification

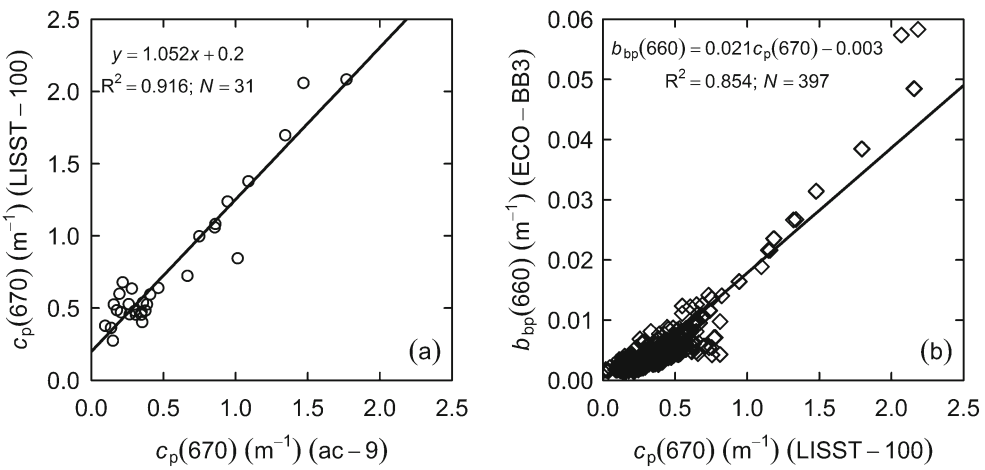

Fig. 2 **a** Plot of $c_p(670)$ measured with the LISST-100 versus $c_p(670)$ measured with the ac-9 at 0.25 m depth; ac-9 values were obtained by linear interpolation between $c_p(630)$ and $c_p(715)$. **b** Plot of $b_{bp}(660)$ measured with the ECO-BB3 versus $c_p(670)$ measured with the LISST-100 for the whole dataset (0–10 m; *solid lines* linear least-squares regressions)

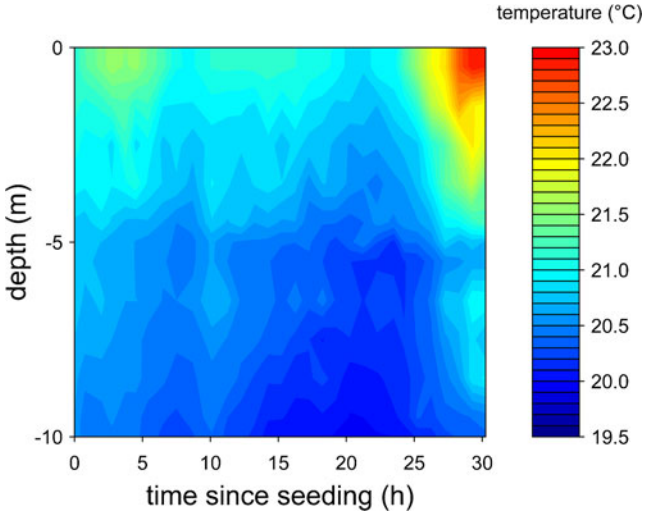

Fig. 3 Temporal variation in seawater temperature measured inside the mesocosm with the LISST-100 sensor during the first 31 h of the experiment

would not measurably affect the sinking of small-sized particles according to Stokes' law.

'Particulate event'

Figure 4 shows the temporal evolution of the three measured optical parameters $b_{bp}(660)$, $c_p(670)$ and $c_p(715)$ within the 0–10 m depth layer of the mesocosm. Only data recorded during the first 31 h after seeding are shown here, in order to focus on rapid processes involved in particulate export. Along with these optical measurements, $V(D)$ and $N(D)$ measured at 0.5, 5.5 and 9.5 m depths are presented (Fig. 5) in order to investigate PSD evolution.

Clear waters

The initial optical properties of the water column were typical of clear waters: $b_{bp}(660)$, $c_p(670)$ and $c_p(715)$ of $1.80\pm0.03\times10^{-3}$, $6\pm4\times10^{-2}$ and $5\pm2\times10^{-2}$ m^{-1} respectively. These values were homogeneous from 0 to 10 m depth, and very similar to those measured outside the mesocosm. These outside values exhibited constant values during the experiment, confirming that the change of optical properties in the mesocosm was indeed due to seeding (cf. outside b_{bp} values given in Fig. 6).

Saharan dust

Maximum particulate attenuation and backscattering coefficients were recorded within the subsurface water layer immediately after seeding. The input of 41.5 g of Saharan dust leads to proportional increases in optical parameters by factors of 32 to 37 at 0.5 m depth. An increase in $V(D)$ and $N(D)$ was also observed at 0.5 m depth ($V(D)$ peaked at 16.3 μm), whereas very low concentrations were measured at 5.5 and 9.5 m depths (Fig. 5a, b). Although the Saharan dust had a volume median diameter of about 6.5 μm, particles

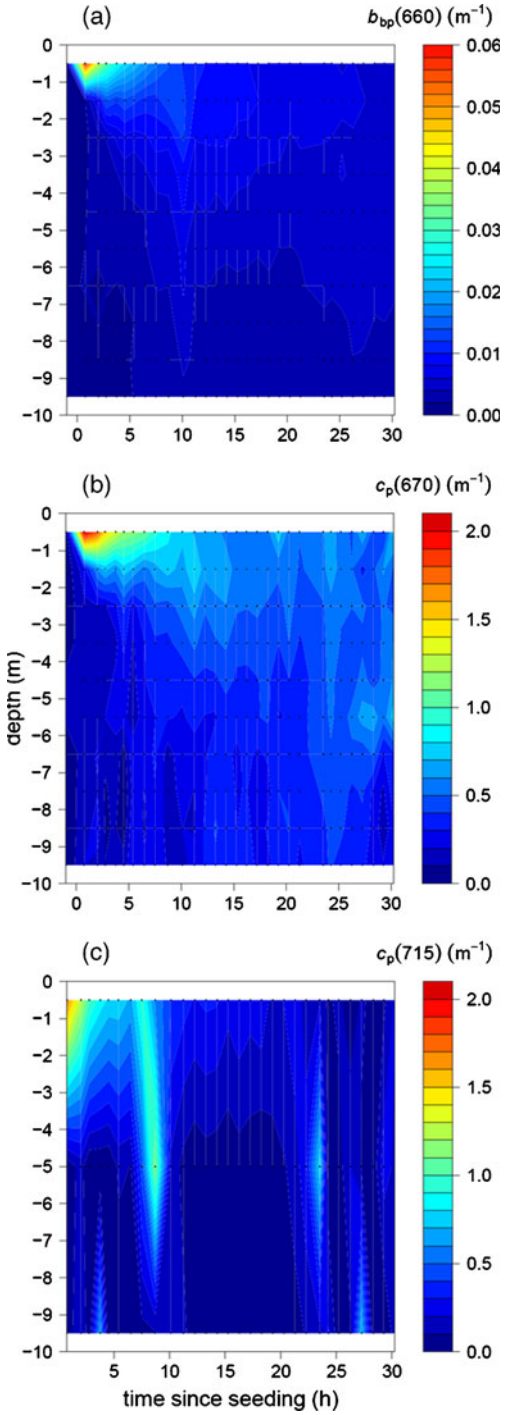

Fig. 4 Temporal and depth variations (0–10 m) of **a** $b_{bp}(660)$ measured with the ECO-BB3, **b** $c_p(670)$ measured with the LISST-100 and **c** $c_p(715)$ measured with the ac-9. Note that ac-9 measurements were conducted only at 0.25, 5 and 10 m depths, and the data then interpolated between 0.25 and 10 m; both ECO-BB3 and LISST data were recorded continuously from 0 to 10 m depth

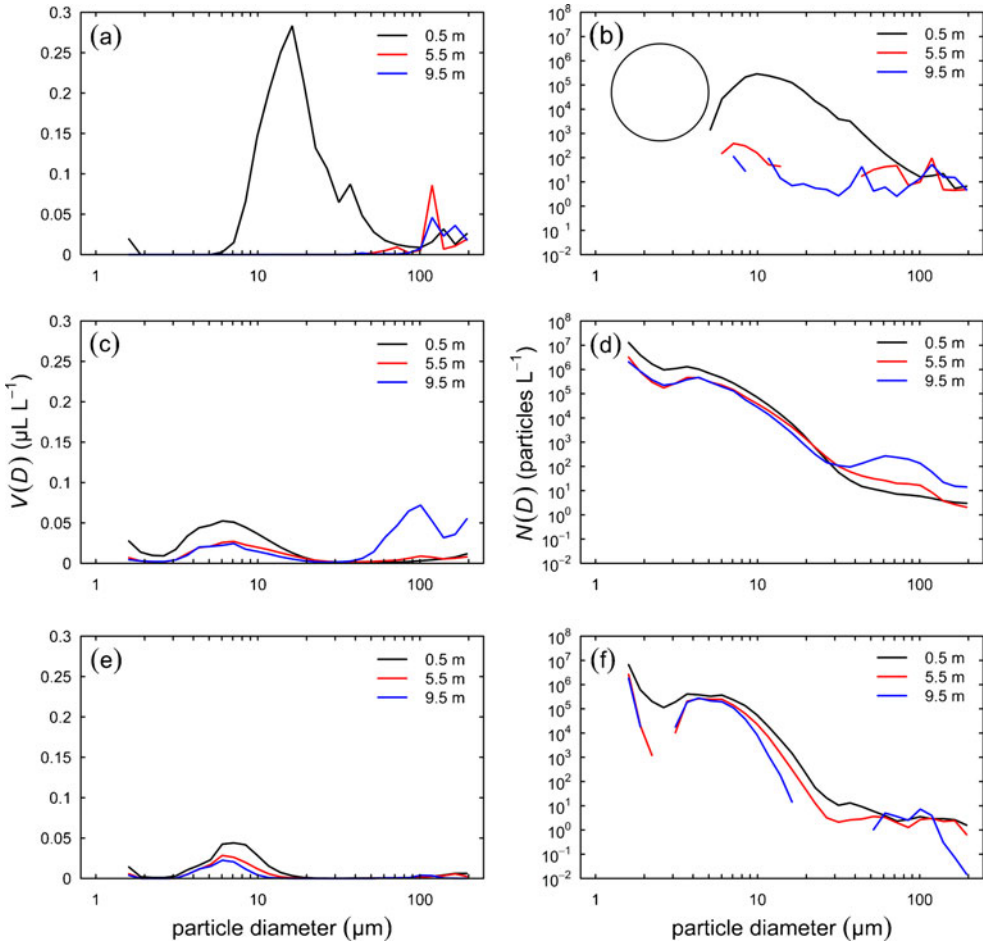

Fig. 5 Volume concentrations of particles $V(D)$ (**a**, **c**, **e**) and corresponding particle number concentrations $N(D)$ (**b**, **d**, **f**) measured 0.75 h (**a**, **b**), 13.25 h (**c**, **d**) and 19.25 h (**e**, **f**) after seeding at 0.5, 5.5 and 9.5 m depths with the LISST-100. *Large circle* on **b** Ambient light contamination of near-forward scattering measurements observed during the daytime (0.75 h after seeding) for the largest scattering angle; the other PSDs were recorded during the night

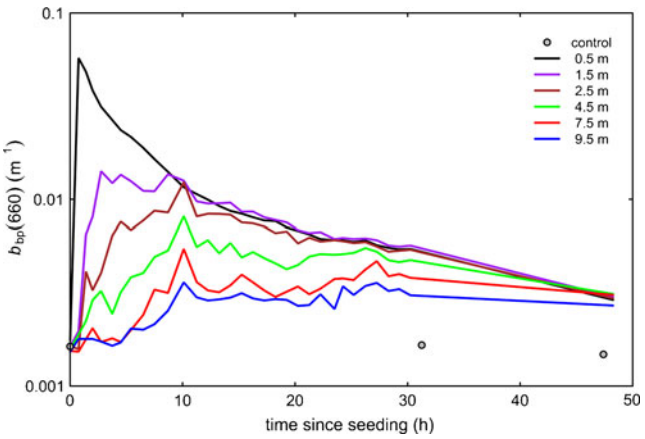

Fig. 6 Plot of $b_{bp}(660)$ at 0.5, 1.5, 2.5, 4.5, 7.5 and 9.5 m depths inside and outside (control) the mesocosm as a function of time after seeding. In this study, b_{bp} serves as proxy of Saharan dust concentration. Note the logarithmic y axis

smaller than 7.11 µm were not observed 0.75 h after seeding. This measurement performed during the daytime (midday) revealed a contamination of the near-forward scattering measurements by ambient red light (cf. large circle on Fig. 5b). This LISST artefact has already been observed in the past. Indeed, by using a LISST modified with a 532 nm laser to measure PSDs in subsurface coastal waters, Reynolds et al. (2010) demonstrated a significant ambient light contamination confined to the first seven size bins (D<3.2 µm). The contamination of the scattering signal by solar irradiance increased with increasing scattering angle, and the smallest size classes were therefore largely underestimated in the presence of ambient solar light.

Particulate export

After the artificial seeding, similar patterns were obtained from the three different optical sensors, enabling us to highlight key steps in the particulate export. During the first

5 h of the experiment, the subsurface values of b_{bp} and c_p decreased suggesting a decrease in SPM concentration in the subsurface and a slight increase in $c_p(670)$ and $c_p(715)$ occurred in deeper layers (Fig. 4). From 5 h after seeding, constant background values were recorded at 9.5 m depth, with $b_{bp}(660)$ values higher than 0.002 m^{-1}. This increase is likely due to a small fraction of the particulate pool sinking immediately after seeding and may be attributed to the largest mineral particles self-aggregating or being integrated into larger biogenic aggregates. Analysis of the backscattering ratio tends to confirm the presence of mineral particles at 9.5 m depth at this time point in the experiment (see Discussion).

Thereafter, two major particulate events were observed. At hour 10 after seeding, distinct increases in $b_{bp}(660)$ and $c_p(715)$ at all depths suggest rapid particle sinking (Fig. 4). Based on $c_p(715)$ data, this event corresponds to the highest particle fluxes recorded during the experiment ($c_p(715)$= 1.20±0.03 m^{-1} at 5 m depth). The PSDs recorded 13.25 h after seeding indicate the presence of two major populations of particles (Fig. 5c, d). One population observed mainly at 0.5 m depth peaked at 6.03 μm, which would correspond to dust particles not yet exported. The other population (diameters centred at D=101 μm) was observed at 5.5 and 9.5 m depths, suggesting the formation and export of larger aggregates. The characteristic shape of particle size distributions in natural waters would show a rapid decrease in particle number concentration with increasing particle diameter. Such a shape was not observed several hours after seeding (Fig. 5f) because of a higher proportion of large particles (>31.6 μm), suggesting that the aggregates were still present.

The second particulate event occurred ~25–30 h after seeding and involved a population of particles with low settling velocities. It corresponds to the maximum $c_p(670)$ value measured at 9.5 m depth (0.41±0.03 m^{-1}) and was detected also by the two other sensors. At hour 31 after seeding, the three optical parameters still had values higher than the initial and control values, with homogenization throughout the water column.

Saharan dust trend

In Fig. 6, $b_{bp}(660)$ is expressed as a function of time at different depths during the two consecutive days of measurements. After an abrupt increase during the first post-seeding hour, the decrease in b_{bp} at 0.5 m depth followed a power law (exponent of −0.7351, R^2=0.984; not shown on Fig. 6). Whereas a main flux of mineral particles rapidly reached 1.5 and 2.5 m depths (~3 h), maximum values of b_{bp} between 4.5 and 9.5 m depths were recorded only 10 h after seeding.

From that time on, b_{bp} values were similar within the upper 2.5 m of the mesocosm and decreased, while a relatively constant flux of particles occurred in deeper layers (4.5–9.5 m) until complete homogenization of the 0–10 m layer was observed 48 h after seeding (note that no measurements were performed between 31 and 48 h). Two days after seeding, b_{bp} values were still 1.8 times higher on average than initial values. The particulate backscattering coefficient varied by more than one order of magnitude inside the mesocosm, whereas outside the mesocosm control values revealed constant optical properties of the water column. The coefficient of variation for $b_{bp}(660)$ in the 0–10 m layer outside the mesocosm during the experimental period was only 7%, with a mean value of 1.5×10^{-3} m^{-1}. This suggests that modifications in optical properties of water inside the mesocosm 2 days after seeding resulted from physicochemical modifications induced by the simulated Saharan dust event.

Discussion and conclusions

On a very short timescale, the experiment mimicked a strong Saharan dust event depositing on surface waters and containing a high variety of living and nonliving particles. How can water optical properties help to understand the fate of such particles during their transfer to the deep ocean? As the measured light attenuation was due mainly to particle scattering at 670 nm in this study (see Materials and methods), the $b_{bp}(660)/c_p(670)$ ratio can serve in distinguishing organic-rich particle assemblages from those dominated by inorganic material. Indeed, inorganic mineral particles have high refraction indices relative to organic particles such as phytoplankton and detrital material characterised by high water content. Seeing that light backscattering is more sensitive to the index of refraction than is the beam attenuation, a high ratio

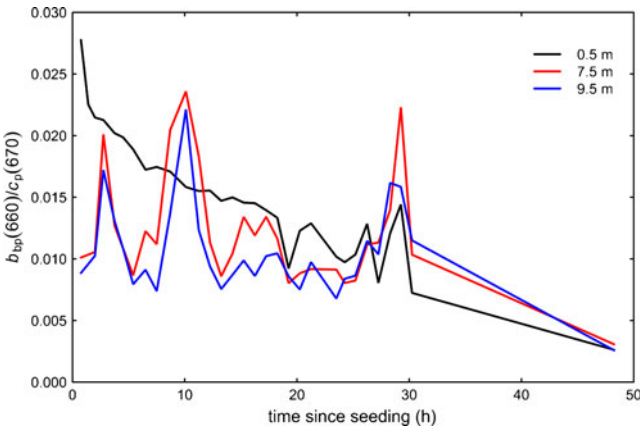

Fig. 7 Plot of $b_{bp}(660)/c_p(670)$ ratio at 0.5, 7.5 and 9.5 m depths as a function of time after seeding. Ratios of 0.03 and 0.005 are typical of mineral and organic particles respectively

corresponds to a predominance of inorganic material, the reverse being the case for organic particles (Twardowsky et al. 2001). Figure 7 illustrates the evolution of this ratio as a function of time at 0.5, 7.5 and 9.5 m depths, encompassing the layer just below the surface and the deeper part of the mesocosm close to the sediment trap.

Rapid change in composition of particle assemblage

The observed backscattering ratios ranged between 0.0026 and 0.0277 (Fig. 7). Similar ranges were observed by Twardowsky et al. (2001) in the Gulf of California (0.002–0.03) and by Boss et al. (2004) in the Mid-Atlantic Bight (0.005–0.035); Westberry et al. (2010) found a median value of 0.010±0.002 (at 526 nm) in the Mediterranean Sea. This large dynamic range encountered in the mesocosm is governed by subsurface variability in this ratio with transition from a clear dominance of mineral particles just after seeding ($b_{bp}(660)/c_p(670)=0.0277$) to a dominance of organic matter (OM) 2 days after seeding ($b_{bp}(660)/c_p(670)=0.0026$). This decrease in backscattering ratio confirms the rapid transfer of mineral particles towards the deeper part of the mesocosm and also reveals an increasing proportion of organic matter likely induced by a fertilization effect of the dust input (see below).

Rapidly settling particle population

An increase in backscattering ratio was observed at depth during the first 5 h of the experiment—$b_{bp}(660)/c_p(670)>0.017$ (Fig. 7). This value is expected for mineral-rich particles (e.g. McKee and Cunningham 2006). For example, Loisel et al. (2007) reported a mean backscattering ratio of 0.0138±0.0083 for the eastern English Channel and southern North Sea, these being typical coastal waters characterised by high mineral matter concentrations. Therefore, this increase in backscattering ratio suggests rapid sinking (~3.6 m h^{-1}) of at least part of the mineral particles introduced. Maximum values of the backscattering ratio at 7.5 and 9.5 m depths were observed 10 h after seeding, corresponding to a settling velocity of ~1 m h^{-1}. This range of settling velocities (~0.27−1 mm s^{-1}) has been reported also for other environments and corresponds to large aggregates (Curran et al. 2007), as observed at 5.5 and 9.5 m depths 13.25 h after seeding in the present study (Fig. 5c, d). These increases in backscattering ratio during the first 10 h indicate that the initial step of particulate export involved mineral particles. Because the backscattering ratio obscures the effect of concentration, however, the importance of this fast mineral export cannot be calculated in terms of actual flux.

Interactions with organic matter

About 20–25 h after seeding, the backscattering ratio was relatively low (<0.01; Fig. 7) at 7.5 and 9.5 m depths, while it decreased continuously within subsurface waters. However, particulate attenuation coefficients measured at 670 and 715 nm demonstrate that particulate export occurred in this time interval (Fig. 4b, c). The backscattering ratio also depends on the relative proportion between small- and large-sized particles, b_{bp} being more sensitive to smallest particles than is c_p (Morel and Ahn 1991; Stramski and Kiefer 1991). Thereby, an increase in the proportion of large particles leads to a decrease in backscattering ratio (Ulloa et al. 1994). Furthermore, this ratio varies inversely with the POC/SPM ratio (Boss at al. 2009). Consequently, the decrease in backscattering ratio suggests a higher proportion of organic material, and may also be the result of the formation of larger particles (Fig. 5f) by aggregation with 'freshly' produced OM. Indeed, mineral

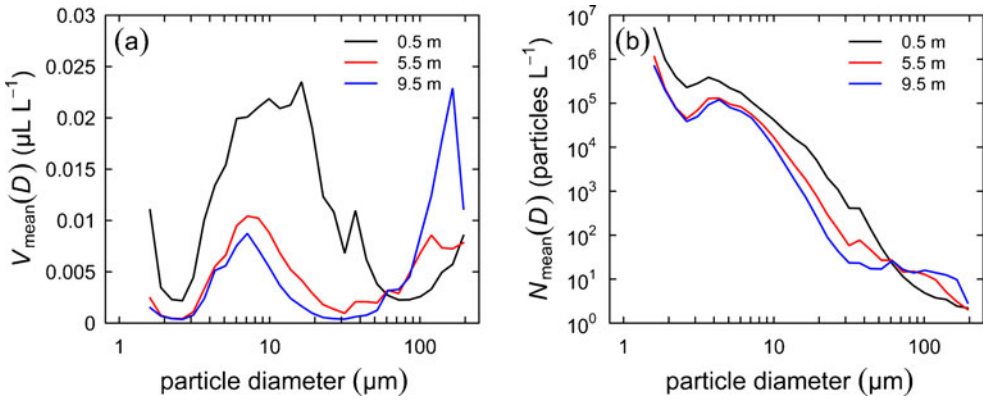

Fig. 8 **a** Mean particle volume concentrations $V_{mean}(D)$ and **b** corresponding mean particle number concentrations $N_{mean}(D)$ at 0.5, 5.5 and 9.5 m depths (calculated as the average of $V(D)$ and $N(D)$ measured after seeding during each profile run (0.75 to 53.25 h after seeding). Because of the high sampling frequency (every hour), some particle size ranges could be overestimated (particularly the smaller size ranges characterised by low settling velocities)

particles aggregate efficiently with OM and the aggregates can become large in the presence of high concentrations of phytoplankton and associated mucus (Hamm 2002).

This interpretation is supported by biogeochemical data collected in the other seeded mesocosms in the study area, where total chlorophyll a concentrations increased on average by a factor of 3.3 after 24 h (C. Brunet, personal communication). Despite a low spatial resolution due to a discrete sampling technique, ac-9 measurements enabled us to support this interpretation. Indeed, from 20 h after seeding, the light absorption coefficient measured at 440 nm (a wavelength centred on a major phytoplankton absorption peak) increased by a factor of 4.3 within the 0–10 m layer and the contribution of $a_p(440)$ to $c_p(440)$ changed from 20% to 43% ($c_p=a_p+b_p$). The increase in the proportion of absorbing particles is consistent with the occurrence of a phytoplankton bloom induced by the Saharan dust.

Slowly settling particle population

The lower values of the backscattering ratio observed 2 days after seeding at all depths (mean value of 0.0026±0.0002; Fig. 7) are consistent with the dominance of particles of low refractive indexes such as phytoplankton and organic detritus. At the end of the measurements, organic matter clearly dominated the particle assemblage but mineral particles were still exported ~30 h after seeding (cf. increase in backscattering ratio; Fig. 7), and part of the mineral particle pool was still in suspension in the water column 2 days after seeding ($b_{bp}(660)$ still higher than initial conditions; Fig. 6).

Integrated trends

To integrate these trends of different particle populations, mean particle volume ($V_{mean}(D)$; Fig. 8a) and mean particle number ($N_{mean}(D)$; Fig. 8b) concentrations were calculated as the average of $V(D)$ and $N(D)$ measured at 0.5, 5.5 and 9.5 m depths during the experiment (0.75–53.25 h after seeding). The higher proportion of <61.2 μm particles observed at 0.5 m depth and the increase in >61.2 μm particle concentrations with depth support our interpretations of (1) a longer residence time of smaller particles in subsurface layers and (2) a formation of aggregates (>61.2 μm) from these small particles during their transfer to deeper layers. Whereas total particle volume concentration at 5.5 m depth peaked at ~120 μm, at 9.5 m depth this was at 165 μm (Fig. 8a), implying that particle aggregation was occurring between 5 and 10 m depths.

These different particle fluxes observed at depth demonstrate that particulate export was a nonlinear multi-step process in the present study. Differently settling particle populations were observed during the experiment. These populations differed in their size distributions and composition. Our approach does not enable us to estimate the actual particle settling velocity because we observed several settling velocity classes. Nevertheless, we can conclude that the fastest settling velocities observed ranged between about 24 and ~86 m day^{-1} and correspond to organic-mineral aggregate populations (>61.2 μm). Taking into account that the particle settling rate increases with depth (Berelson 2002), this range of settling velocities is comparable with in situ measurements for Saharan dust based on sediment trap data. Indeed, after an extreme Saharan dust event (22 g m^{-2}), Ternon et al. (2010) recorded a minimum settling velocity of 100 m day^{-1} (sediment traps at 1,000 m). Brust et al. (2011) reported net settling velocities (including atmospheric deposition) ranging between 32 and 44 m day^{-1} (sediment traps at 2,000 m), and Neuer et al. (2004) a net settling velocity of 35 m day^{-1} (sediment traps at 500 m).

These observations at high temporal and spatial resolutions of an artificial seeding mimic an actual Saharan dust event in very clear Mediterranean waters, and provide a new insight of processes occurring in the surface ocean. Optical measurements indicate that particulate export is affected by the formation of organic-mineral aggregates. This process, which occurred within the upper few meters of the water column, depends mainly on the quantity and quality of OM (Passow and De La Rocha 2006). The fertilization induced by the first seeding had changed the characteristics of the water column with the appearance of 'freshly' produced OM. A companion dataset integrating biogeochemical data (such as POC/SPM in sediment traps) along with results from a second seeding (7 days after this experiment in the same mesocosm) addresses the role of organic matter in particle aggregation and, therefore, in particulate export in more detail.

Acknowledgements Matthieu Bressac acknowledges a grant provided by the ACRI-ST company and the French National Association for Research and Technology (ANRT). This work was funded by the ANR DUNE project under contract ANR-07-BLAN-0126-01. Francis Louis is thanked for his help in the conception of the 'optical' mesocosm and Orens Pasqueron De Fommervault for assistance in the preparation of the campaign. Thibaut Wagener, Christophe Brunet and Karine Desboeufs are greatly acknowledged for their help in field measurements. The authors thank Céline Ridame and Christophe Brunet for providing salinity and chlorophyll data respectively. This field campaign could not have taken place without the logistical support and facilities of the Parc Naturel Régional de Corse, and the diving expertise of David Luquet and Christian Rouvière from the Observatoire Océanologique de Villefranche. We warmly thank Alina Ebling who kindly polished the English and two anonymous reviewers for their constructive suggestions.

References

Agrawal YC, Pottsmith HC (2000) Instrument for particle size and settling velocity observations in sediment transport. Mar Geol 16:89–114. doi:10.1016/S0025-3227(00)00044-X

Agrawal YC, Whitmire A, Mikkelsen OA, Pottsmith HC (2008) Light scattering by random shaped particles and consequences on measuring suspended sediments by laser diffraction. J Geophys Res 113:C04023. doi:10.1029/2007JC004403

Berelson WM (2002) Particle settling rates increase with depth in the ocean. Deep-Sea Res II 49:237–251. doi:10.1016/S0967-0645(01)00102-3

Bonnet S, Guieu C, Chiaverini J, Ras J, Stock A (2005) Effect of atmospheric nutrients on the autotrophic communities in a low nutrient, low chlorophyll system. Limnol Oceanogr 50(6):1810–1819. doi:10.4319/lo.2005.50.6.1810

Boss E, Pegau WS (2001) Relationship of light scattering at an angle in the backward direction to the backscattering coefficient. Appl Optics 40:5503–5507. doi:10.1364/AO.40.005503

Boss E, Pegau WS, Lee M, Twardowski M, Shybanov E, Korotaev G, Baratange F (2004) Particulate backscattering ratio at LEO 15 and its use to study particle composition and distribution. J Geophys Res 109:C01014. doi:10.1029/2002JC001514

Boss E, Slade W, Hill P (2009) Effect of particulate aggregation in aquatic environments on the beam attenuation and its utility as a proxy for particulate mass. Opt Express 17(11):9408–9420. doi:10.1364/OE.17.009408

Brust J, Schulz-Bull DE, Leipe T, Chavagnac V, Waniek JJ (2011) Descending particles: from the atmosphere to the deep ocean – A time series study in the subtropical NE Atlantic. Geophys Res Lett 38:L06603. doi:10.1029/2010GL045399

Buat-Ménard P, Davies PJ, Remoudaki E, Miquel JC, Bergametti G, Lamber CE, Ezat E, Quétel CR, La Rosa J, Fowler SW (1989) Non-steady-state biological removal of atmospheric particles from Mediterranean surface waters. Nature 340:131–133. doi:10.1038/340131a0

Curran KJ, Hill PS, Milligan TG, Mikkelsen OA, Law BA, Durrieu de Madron X, Bourrin F (2007) Settling velocity, effective density, and mass composition of suspended sediment in a coastal bottom boundary layer, Gulf of Lions, France. Cont Shelf Res 27:1408–1421. doi:10.1016/j.csr.2007.01.014

De La Rocha CL, Nowald N, Passow U (2008) Interactions between diatom aggregates, minerals, particulate organic carbon, and dissolved organic matter: further implications for the ballast hypothesis. Global Biogeochem Cy 22:GB4005. doi:10.1029/2007GB003156

Guieu C, Dulac F, Desboeufs K, Wagener T, Pulido-Villena E, Grisoni JM, Louis F, Ridame C, Blain S, Brunet C, Bon Nguyen E, Tran S, Labiadh M, Dominici JM (2010) Large clean mesocosms and simulated dust deposition: a new methodology to investigate responses of marine oligotrophic ecosystems to atmospheric inputs. Biogeosciences 7:2765–2784. doi:10.5194/bg-7-2765-2010

Hamm CE (2002) Interactive aggregation and sedimentation of diatoms and clay-sized lithogenic material. Limnol Oceanogr 47(6):1790–1795. doi:10.4319/lo.2002.47.6.1790

Langford VS, McKinley AJ, Quickenden TI (2001) Temperature dependence of the visible-near-infrared absorption spectrum of liquid water. J Phys Chem A 105(39):8916–8921. doi:10.1021/jp010093m

Loisel H, Morel A (1998) Light scattering and chlorophyll concentration in case 1 waters: a reexamination. Limnol Oceanogr 43(5):847–858. doi:10.4319/lo.1998.43.5.0847

Loisel H, Mériaux X, Berthon JF, Poteau A (2007) Investigation of the optical backscattering to scattering ratio of marine particles in relation to their biogeochemical composition in the eastern English Channel and southern North Sea. Limnol Oceanogr 52(2):739–752. doi:10.4319/lo.2007.52.2.0739

Loÿe-Pilot MD, Martin JM (1996) Saharan dust input to the Western Mediterranean: an eleven years record in Corsica. In: Guerzoni S, Chester R (eds) The impact of desert dust across the Mediterranean. Kluwer, Dordrecht, pp 191–199

Maring H, Savoie DL, Izaguirre MA, Custals L, Reid JS (2003) Mineral dust aerosol size distribution change during atmospheric transport. J Geophys Res 108(D19):8592. doi:10.1029/2002JD002536

McKee D, Cunningham A (2006) Identification and characterisation of two optical water types in the Irish Sea from in situ inherent optical properties and seawater constituents. Estuarine Coastal Shelf Sci 68:305–316. doi:10.1016/j.ecss.2006.02.010

Morel A (1974) Optical properties of pure water and pure seawater. In: Jerlov NG, Steeman Nielsen E (eds) Optical aspects of oceanography. Academic Press, New York, pp 1–24

Morel A, Ahn YH (1991) Optics of heterotrophic nanoflagellates and ciliates: a tentative assessment of their scattering role in oceanic waters compared to those of bacterial and algal cells. J Mar Res 49:177–202. doi:10.1357/002224091784968639

Neuer S, Torres-Padrón ME, Gelado-Caballero MD, Rueda MJ, Hernández-Brito J, Davenport R, Wefer G (2004) Dust deposition pulses to the eastern subtropical North Atlantic gyre: does ocean's biogeochemistry respond? Global Biogeochem Cy 18:GB4020. doi:10.1029/2004GB002228

Passow U, De La Rocha CL (2006) Accumulation of mineral ballast on organic aggregates. Global Biogeochem Cy 20:GB1013. doi:10.1029/2005GB002579

Pegau WS, Deric G, Zaneveld JRV (1997) Absorption and attenuation of visible and near-infrared light in water: dependence on temperature and salinity. Appl Optics 36(24):6035–6046. doi:10.1364/AO.36.006035

Ploug H, Iversen MH, Fisher G (2008) Ballast, sinking velocity, and apparent diffusivity within marine snow and zooplankton fecal pellets: implications for substrate turnover by attached bacteria. Limnol Oceanogr 53(5):1878–1886. doi:10.4319/lo.2008.53.5.1878

Ploug H, Terbrüggen A, Kaufmann A, Wolf-Gladrow D, Passow U (2010) A novel method to measure particle sinking velocity in vitro, and its comparison to three other in vitro methods. Limnol Oceanogr Meth 8:386–393. doi:10:4319/lom.2010.8.386

Reynolds RA, Stramski D, Wright VM, Wozniak SB (2010) Measurements and characterization of particle size distributions in coastal waters. J Geophys Res 115:C08024. doi:10.1029/2009JC005930

Stramski D, Kiefer DA (1991) Light scattering by microorganisms in the open ocean. Prog Oceanogr 28:343–383. doi:10.1016/0079-6611(91)90032-H

Sullivan JM, Twardowski MS, Donaghay PL, Freeman SA (2005) Use of optical scattering to discriminate particle types in coastal waters. Appl Optics 44(9):1667–1680. doi:10.1364/AO.44001667

Sullivan JM, Twardowski MS, Zaneveld JRV, Moore CM, Barnard AH, Donaghay PL, Rhoades B (2006) Hyperspectral temperature and salt dependencies of absorption by water and heavy water in the 400–750 nm spectral range. Appl Optics 45(21):5294–5309. doi:10.1364/AO.45.005294

Ternon E, Guieu C, Loÿe-Pilot MD, Leblond N, Bosc E, Gasser B, Miquel JC, Martin J (2010) The impact of Saharan dust on the particulate export in the water column of the North Western Mediterranean Sea. Biogeosciences 7:809–826. doi:10.5194/bg-7-809-2010

Ternon E, Guieu C, Ridame C, L'Helguen S, Catala P (2011) Longitudinal variability of the biogeochemical role of Mediterranean aerosols in the Mediterranean Sea. Biogeosciences 8:1067–1080. doi:10.5194/bg-8-1067-2011

Twardowsky MS, Boss E, Macdonald JB, Pegau WS, Barnard AH, Zaneveld JRV (2001) A model for estimating bulk refractive index from the optical backscattering ratio and the implications for understanding particle composition in case I and case II waters. J Geophys Res 106(C7):14129–14142. doi:10.1029/2000JC000404

Ulloa O, Sathyendranath S, Platt T (1994) Effect of the particle-size distribution on the backscattering ratio in seawater. Appl Optics 33(30):7070–7077. doi:10.1364/AO.33.007070

Westberry TK, Dall'Olmo G, Boss E, Behrenfeld MJ, Moutin T (2010) Coherence of particulate beam attenuation and backscattering coefficients in diverse open ocean environments. Opt Express 18(15):15419–15425. doi:10.1364/OE.18.015419

Zaneveld JRV, Kitchen JC, Moore CC (1994) The scattering error correction of reflecting tube absorption meters. In: Ackleson S (ed) Ocean Optics XII. Proc SPIE 2258, pp 44–55. doi:10.1117/12.190095